Computer-assisted design for atenolol prodrugs for the use in aqueous formulations

Article *in* Journal of Molecular Modeling · July 2011

DOI: 10.1007/s00894-011-1180-7 · Source: PubMed

3 authors, including:

Rafik Karaman
Al-Quds University
233 PUBLICATIONS **2,818** CITATIONS
SEE PROFILE

Khuloud K Dajani
Al-Quds University
12 PUBLICATIONS **149** CITATIONS
SEE PROFILE

Computer-assisted design for atenolol prodrugs for the use in aqueous formulations

Rafik Karaman, Khuloud Dajani & Hussein Hallak

Journal of Molecular Modeling
Computational Chemistry - Life Science - Advanced Materials - New Methods

ISSN 1610-2940
Volume 18
Number 4

J Mol Model (2012) 18:1523-1540
DOI 10.1007/s00894-011-1180-7

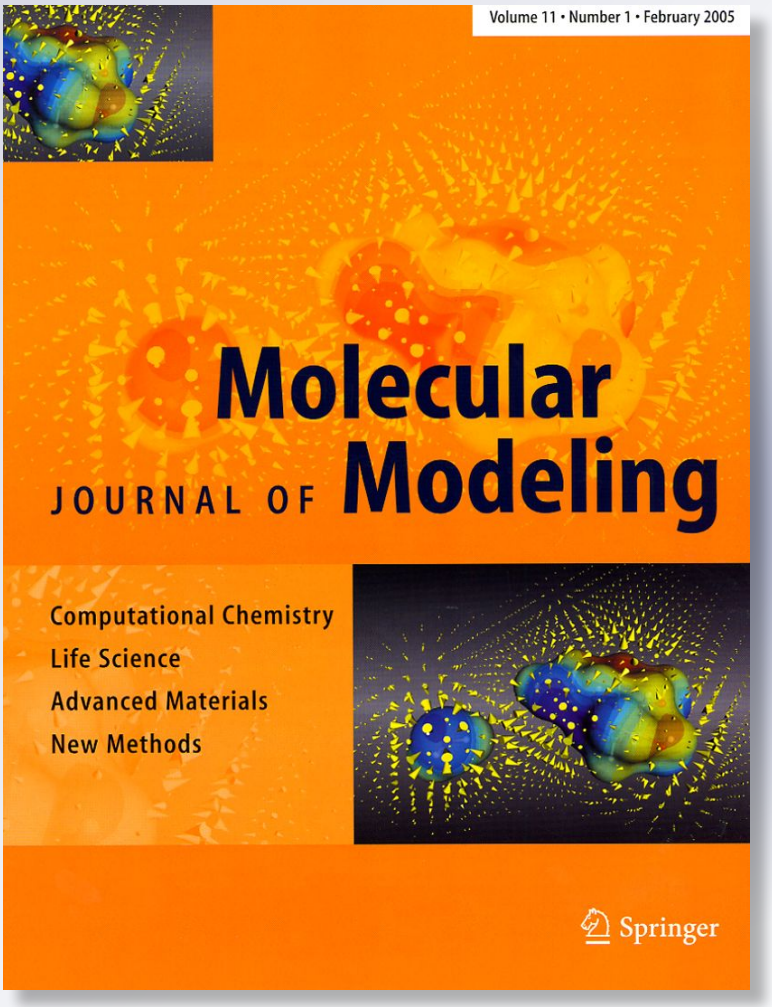

Springer

J Mol Model (2012) 18:1523–1540
DOI 10.1007/s00894-011-1180-7

ORIGINAL PAPER

Computer-assisted design for atenolol prodrugs for the use in aqueous formulations

Rafik Karaman · Khuloud Dajani · Hussein Hallak

Received: 10 May 2011 / Accepted: 4 July 2011 / Published online: 23 July 2011

Abstract Based on stability studies on the drugs atenolol and propranolol and some of their derivatives it is believed that increasing the lipophilicity of the drug will lead to an increase in the stability of its aqueous solutions and will provide a prodrug system with the potential for releasing atenolol in a controlled manner. Using DFT theoretical calculations we have calculated an intramolecular acid catalyzed hydrolysis in nine maleamic (4-amino-4-oxo-2butenoic) acids (Kirby's N-alkylmaleamic acids), **1**–**9**. The DFT calculations confirmed that the acid-catalyzed hydrolysis mechanism in these systems involves: (1) a proton transfer from the hydroxyl of the carboxyl group to the adjacent amide carbonyl carbon, (2) an approach of the carboxylate anion toward the protonated amide carbonyl carbon to form a tetrahedral intermediate; and (3) a collapse of the tetrahedral intermediate into products. Furthermore, DFT calculations in different media revealed that the reaction rate-limiting step depends on the reaction medium. In aqueous medium the rate-limiting step is the collapse of the tetrahedral intermediate whereas in the gas phase the formation of the tetrahedral intermediate is the rate-limiting step. Furthermore, the calculations establish that the acid-catalyzed hydrolysis efficiency is largely sensitive to the pattern of substitution on the carbon-carbon double bond. Based on the experimental $t_{1/2}$ (the time needed for the conversion of 50% of the reactants to products) and EM (effective molarity) values for processes **1**–**9** we have calculated the $t_{1/2}$ values for the conversion of the two prodrugs to the parental drug, atenolol. The calculated $t_{1/2}$ values for **ProD 1**–**2** are predicted to be 65.3 hours and 11.8 minutes, respectively. Thus, the rate by which atenolol prodrug undergoes cleavage to release atenolol can be determined according to the nature of the linker of the prodrug (Kirby's N-alkylmaleamic acids **1–9**).

Keywords Amide hydrolysis · Anti-hypertensive agents · Atenolol prodrugs · DFT calculations · Enzyme catalysis · Intramolecular acid-catalyzed hydrolysis · Maleamic acid amide derivatives · Strain effects

Introduction

Atenolol [4-(2-hydroxy-isopropylaminopropoxy)-phenylacetamide], is a cardioselective beta1-adrenergic receptor blocking agent used to lower high blood pressure (hypertension), prevent angina pectoris, treat arrhythmia and to reduce the risk of heart complications following a heart attack. Atenolol works by affecting the response to nerve impulses in certain parts of the body, like the heart. As a result, a slower heart beat and lower blood pressure can be expected. When the blood pressure is lowered, a decrease in the heart oxygen demand is observed [1–8].

Atenolol is available as 25, 50 and 100 mg tablets for oral administration. However, most of these medicines are not formulated for easy or accurate administration to children for the migraine indication or in elderly patients who may have difficulty swallowing tablets. Attempts to prepare a liquid formulation was challenging because

Electronic supplementary material The online version of this article (doi:10.1007/s00894-011-1180-7) contains supplementary material, which is available to authorized users.

R. Karaman (✉) · H. Hallak
Faculty of Pharmacy, Al-Quds University,
Box 20002, Jerusalem, Palestine
e-mail: dr_karaman@yahoo.com

K. Dajani
Faculty of Public Health Sciences, Al-Quds University,
Box 20002, Jerusalem, Palestine

atenolol is unstable in solutions. Studies showed that the degradation rate of atenolol is dependent on the temperature, indicating higher stability at 4 °C. Atenolol syrup is stable only for 9 days. Furthermore, oral doses of atenolol are incompletely absorbed (range 46-62%), even when formulated as a solution. Thus the development of more lipophilic prodrug that is stable in aqueous medium is a significant challenge [1–8].

Pharmacologically inactive chemical derivative that could be used to alter the physicochemical properties of atenolol, in a temporary manner and to increase its usefulness should be lipophilic linker that is covalently linked to the parent drug and can be converted in vivo to the active drug molecule, enzymatically or nonenzymatically, to exert a therapeutic effect. Ideally, the prodrug should be converted to the original drug as soon as the goal is achieved, followed by the subsequent rapid elimination of the released derivatizing group [9–11].

Improvement of atenolol pharmacokinetic absorption properties and hence its effectiveness may increase the absorption of the drug via a variety of administration routes.

To achieve this goal, atenolol prodrugs must possess the following properties: (i) to be readily soluble in a physiological environment (ii) to have a moderate hydrophilic lipophilic balance (HLB) value (iii) to provide upon chemical cleavage the active drug in a controlled manner, and (iv) to furnish upon cleavage a safe and non-toxic by-products. By complying with the four requirements described above the following objectives may be fulfilled: (1) a relatively high absorption of the prodrug into the body tissues. (2) The capability to use the drug in different dosage forms, especially in oral solutions form. (3) A chemically driven sustained release system that releases atenolol in a controlled manner once the prodrug reaches the human blood circulation system; and (4) a drug with physico-chemical properties such that leading to a high bioavailability and efficient pharmacokinetic properties.

Since atenolol is a very hydrophilic molecule with a pKa of 9.6, it undergoes ionization in the stomach and intestine thus its oral bioavailability is low due to inefficient absorption through membranes. Approximately 50% of an oral dose is absorbed from the gastrointestinal tract, the remainder being excreted unchanged in the feces. Unlike propranolol or metoprolol, but like nadolol, atenolol undergoes little or no metabolism by the liver, and the absorbed portion is eliminated primarily by renal excretion. Note the log P (partition coefficient) for atenolol is 0.5. Hence, design and synthesis of a relatively more lipophilic prodrugs that can provide the parental drug in a sustained release manner might result in a better clinical outcome, more convenient dosing regimens and potentially less side effects [1–8].

Recently we have been studying the mechanisms for a number of intramolecular processes that have been utilized as enzyme models and lately as prodrug linkers [12–30]. Using different molecular orbital methods such as DFT and ab initio at various levels, we have researched: (a) S_N2-based-cyclization reactions of di-carboxylic semi-esters as studied by Bruice [31, 32] (b) acid-catalyzed lactonization of hydroxy-acids as investigated by Cohen [33–35] and Menger [36–43], (c) intramolecular S_N2-based cyclization reactions as explored by Brown's group [44] and Mandolini's group [45], (d) proton transfer between two oxygens in Kirby's acetals [46–55], and proton transfer between nitrogen and oxygen in Kirby's enzyme models [46–55], (e) proton transfer between two oxygens in rigid systems as investigated by Menger [36–43], and (f) proton transfer from oxygen to carbon in some of Kirby's enol ethers [46–55]. These studies revealed the following: (1) rate enhancement in intramolecular processes is due to both entropy and enthalpy effects. In the cases by which enthalpic effects were predominant such as in cyclization reactions, steric effects was the cause for the accelerations, whereas proximity orientation was the dominant factor in the cases of proton transfer reactions. (2) The reaction type intermolecular or intramolecular is determined on the distance between the two reacting centers. In the cases by which the distance between the two reactive centers exceeds 3 Å an intermolecular reaction is preferred due to the feasibility of engagement of a water molecule (solvent) whereas, an intramolecular process is preferable when the distance between the electrophile and nucleophile is less than 3 Å. (3) The *gem*-dialkyl effect in S_N2-based ring-closing reactions leading to three-, four- and five-membered rings is dominant in those involving the formation of five-membered ring, and the need for directional flexibility decreases as the size of the ring being formed increases. (4) The efficiency of proton transfer between two oxygens and between nitrogen and oxygen in Kirby's acetal systems is due to a strong hydrogen bonding developed in the products and the corresponding transition states leading to them [12–33].

We have concluded from our recent studies on intramolecularity that there is a necessity to explore the reaction mechanism in order to assign the factors affecting the reaction rate for a design of an efficient chemical device to be used as prodrug linker capable of librating the parental drug in a controlled manner [12–33]. The prodrugs are designed such that they have the potential to undergo cleavage reactions in physiological environments (stomach at pH 1.5, intestine at pH 6.5 or/and blood circulation at pH 7.4) with rates that are dependent on the structural features of the pharmacologically inactive linker. Different linkers could be used to obtain a number of prodrugs with the capability to release the parental drug in

various rates that are depending on the nature or the structural features of the linker.

Continuing our study for utilizing intramolecularity to design potential linkers for amine drugs, we sought to study the mechanism and driving forces affecting the acid-catalyzed hydrolysis rate in some of Kirby's acid amides (prodrugs linkers) [56, 57]. It is expected that such linkers might have a potential to be good carriers to the anti-hypertensive agent, atenolol.

Our proposed atenolol prodrugs based on acid-catalyzed cyclization reactions of amide acids are depicted in Scheme 1.

As shown in Scheme 1, the only difference between atenolol prodrugs and the parental drug, atenolol, is that the former has an amide moiety instead of the free amine group in the latter. By doing so the alcohol derivative thus formed (prodrug) will be much more stable than the corresponding amino alcohol, atenolol, due to general chemical stability for tertiary alcohols when compared to amine alcohols. Further, stability studies on ester derivatives of atenolol have showed that the ester derivatives are much more stable than the corresponding alcohol, atenolol, when they are formulated in aqueous solutions. In addition, kinetic studies on the drugs atenolol and propranolol revealed that increasing the lipophilicity of the drug leads to an increase in the stability of its aqueous solutions. Based on the above it is expected that atenolol prodrugs shown in Scheme 1 will be more resistant to heat or/oxidation when standing in aqueous solutions [1–8].

Based on the DFT calculations on the acid-catalyzed hydrolysis of amide acids **1**–**9** reported herein (Scheme 2), two atenolol prodrugs are proposed. As shown in Scheme 1, the atenolol prodrugs, **ProD 1** and **ProD 2**, have a carboxylic acid group (hydrophilic moiety) and a lipophilic moiety (the rest of the molecule), where the combination of both groups ensures a moderate HLB. It should be noted that the HLB value of the prodrug moiety will be determined upon the physiologic environment by which the prodrug is dissolved. For example, in the stomach, the atenolol prodrugs will primarily exist in the carboxylic acid form whereas in the blood circulation the carboxylate anion form will be predominant. It is planned that **ProD 1–2** (Scheme 1) will be obtained as sodium or potassium carboxylate salts since this form is expected to be stable in aqueous medium.

In this manuscript, we report a computational study which revealed the mechanism for intramolecular acid catalyzed hydrolysis of maleamic (4-amino-4-oxo-2butenoic) acids (Kirby's N-alkylmaleamic acids) **1**–**9** (Scheme 2). In addition, based on the rates for processes **1**–**9**, the calculated $t_{1/2}$ values for **ProD 1–2** were predicted.

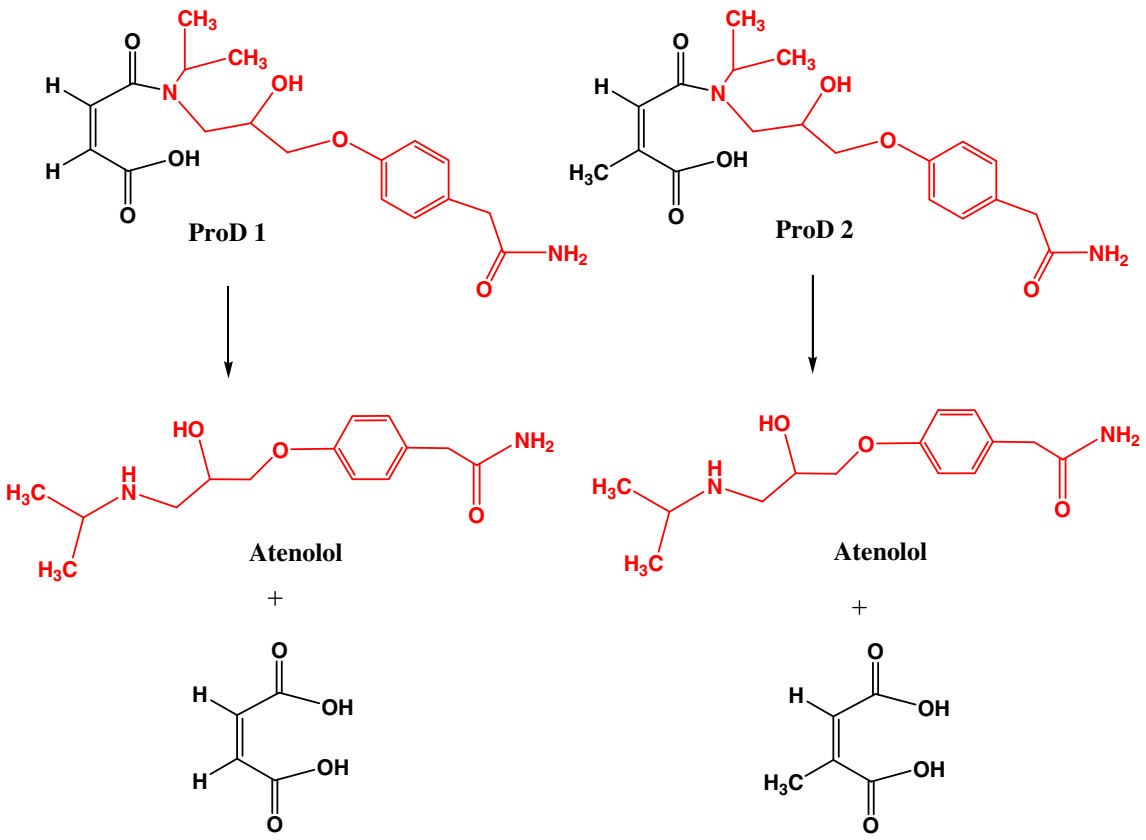

Scheme 1 Chemical structures for atenolol prodrugs **ProD1-2**

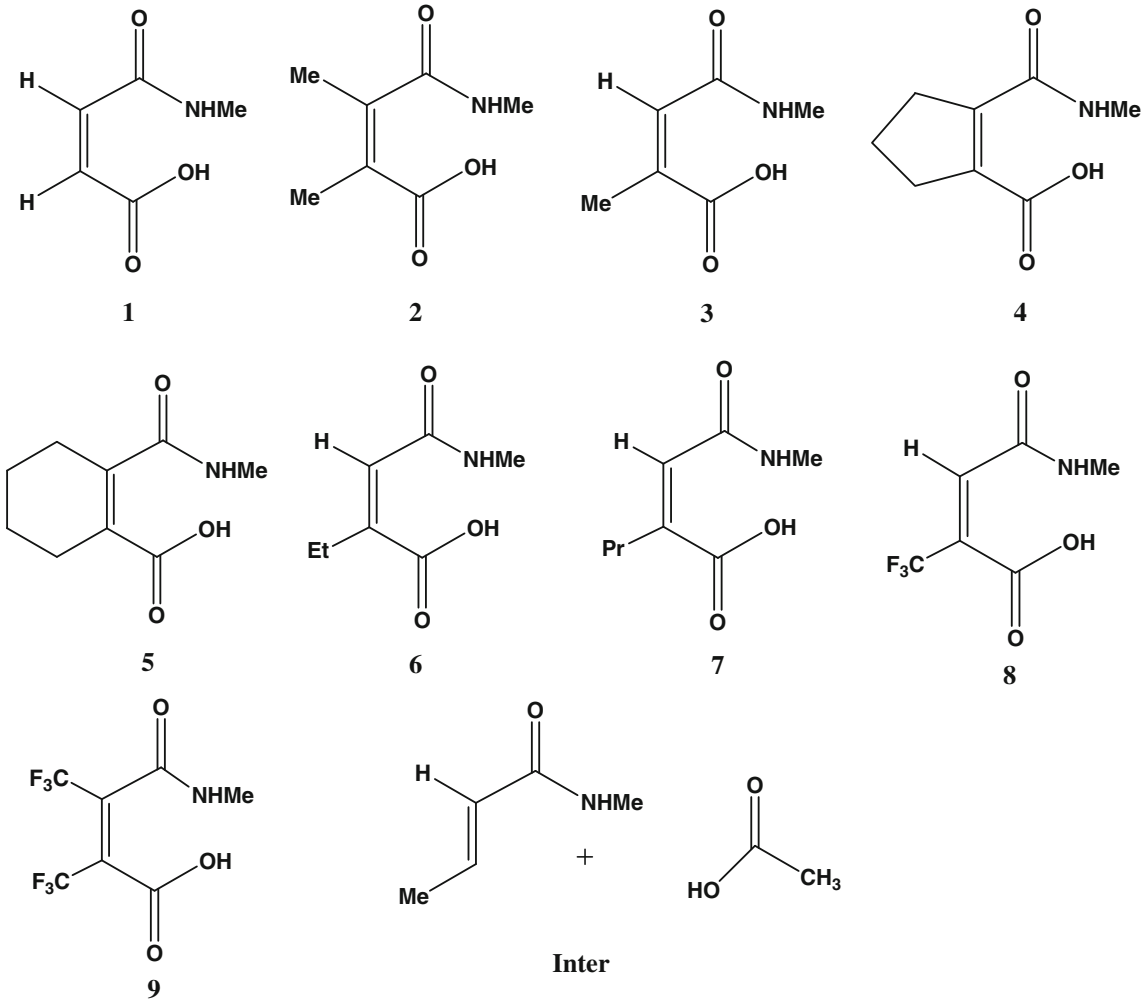

Scheme 2 Chemical structures for maleamic acid derivatives 1–9 and Inter

The goals of this work were to: (1) calculate all possible mechanistic routes for the reactions of **1**–**9** and to unravel the nature of the force(s) affecting the rate as a function of substitution on the carbon-carbon double bond, (b) design of atenolol prodrugs that are relatively stable in aqueous solutions and have the capability to undergo cleavage reaction in physiological environment to furnish atenolol in a controlled manner.

Calculation methods

The Becke three-parameter, hybrid functional combined with the Lee, Yang, and Parr correlation functional, denoted B3LYP, were employed in the calculations using density functional theory (DFT). Calculations were carried out based on the restricted Hartree-Fock method and were run using the quantum chemical package Gaussian-98 [58]. The starting geometries of all the molecules were obtained using the Argus Lab program [59] and were initially optimized at the HF/6-31 G level in the presence of one molecule of water, followed by optimization at the B3LYP/6-31 G(d,p) level [58]. Total geometry optimizations included all internal rotations. Second derivatives were estimated for all three N-6 geometrical parameters during optimization. The search for the global minimum structure in each of the systems studied was accomplished by 360° rotation of the carboxylic group about the bond C6-C7 (i.e., variation of the dihedral angle O1C7C6C5, Chart 1), and 360° rotation of the carbonyl amide group about the bond C4-C5 (i.e., variation of the dihedral angle O3C4C5C6) in increments of 10° and calculation of the conformational energies (see Chart 1). In the DFT calculations for **1**–**9** and **ProD 1**–**2**, two types of conformations in particular were considered: one in which the amide carbonyl is *syn* to the carboxyl group and another in which it is *anti*. An energy minimum (a stable compound or a reactive intermediate) has no negative vibrational force constant. A transition state is a saddle point which has only one negative vibrational force constant [60]. Transition states were located first by the normal reaction coordinate method [61] where the enthalpy

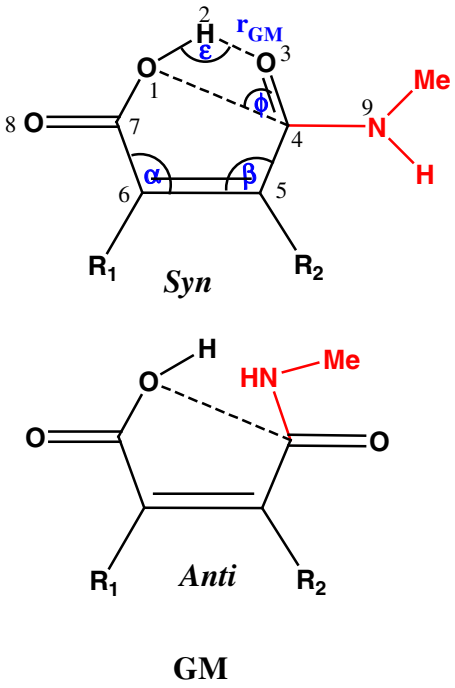

Chart 1 Representation of an acid-catalyzed hydrolysis in Kirby's acid amides **1**–**9**. GM is the global minimum structure. r_{GM} and r_{AP} are the hydrogen bond distance and the approach distance, respectively. α, β, ε and ρ are bond angles

changes was monitored by stepwise changing the interatomic distance between two specific atoms. The geometry at the highest point on the energy profile was re-optimized by using the energy gradient method at the B3LYP/6-31 G (d,p) level of theory [58]. The "reaction coordinate method" [61] was used to calculate the activation energy in maleamic (4-amino-4-oxo-2butenoic) acids (Kirby's N-alkylmaleamic acids), **1**–**9**, **ProD 1**–**2** and **Inter** (Schemes 1 and 2). In this method, one bond length is constrained for the appropriate degree of freedom while all other variables are freely optimized. The activation energy values for the approach processes (the approach of O1 toward C4, Chart 1) were calculated from the difference in energies of the global minimum structures (GM) and the derived transition states (TS_2 in Scheme 3). Similarly, the activation energies of the dissociation processes (the breakdown of C4-N9 bond, Chart 1) were calculated from the difference in energies of the global minimum structures (GM) and the corresponding transition states (TS_4 in Scheme 3). Verification of the desired reactants and products was accomplished using the "intrinsic coordinate method" [61]. The transition state structures were verified by their one negative frequency. Full optimization of the transition states was accomplished after removing any constrains imposed while executing the energy profile. The activation energies obtained from DFT at B3LYP/6-31 G (d,p) level of theory for **1**–**9**, **ProD 1**–**2** and **Inter** were calculated with and without the inclusion of solvent (water and ether). The calculations with the incorporation of a solvent were performed using the integral equation formalism model of the polarizable continuum model (PCM) [62–65].

Results and discussion

Kirby and coworkers have investigated the acid-catalyzed hydrolysis reactions of **1**–**9** (Scheme 2) and have concluded that the amide bond cleavage is due to intramolecular nucleophilic catalysis by the adjacent carboxylic acid group. Based on their kinetic results it was suggested that the rate-limiting step is the one by which dissociation of the tetrahedral intermediate occurs [56]. In 1990, Katagi has theoretically investigated the hydrolysis reaction using AM1 semiempirical method. Katagi's AM1 study revealed that the rate- limiting step is the formation of the tetrahedral intermediate and not its collapse [66]. Since Katagi's theoretical calculations were run in the presence of only two water molecules which resembles somewhat the gas phase environment we sought to study this reaction using Becke three-parameter hybrid functional combined with the Lee, Yang, and Parr correlation functional (B3LYP) methods, which are superior to semiempirical methods, and to run the calculations in the gas phase as well as in other solvents such as ether and a cluster of water due to the importance of the solvent in stabilizing or destabilizing the chemical entities involved in the hydrolysis reaction.

Replacing the N-methyl amide group in **1**–**9** (Scheme 2) with atenolol drug, as shown for **ProD 1** and **ProD 2** in Scheme 1, is not expected to have any significant effect on the relative rates of these processes. Therefore, computational calculations of the kinetic and thermodynamic properties for processes **1**–**9** will shed some light on the rates for the chemical cleavage of prodrugs **ProD 1** and **ProD 2** to the anti-hypertensive drug, atenolol.

In order to utilize systems **1**–**9** as prodrug carriers for atenolol as shown in the cases of **ProD 1**–**2** their mechanism should be unraveled. The suggested mechanism for the acid-catalyzed hydrolysis of **1**–**9** involves proton transfer from the carboxylic group to the adjacent amino carbonyl carbon followed by a nucleophilic attack of the carboxylate anion onto the protonated carbonyl carbon to form tetrahedral intermediate which dissociates to provide products (Scheme 3). In order to determine whether the rate-limiting step in the hydrolysis process is the formation of the tetrahedral intermediate as was suggested by Katagi [66] or its collapse as was proposed by Kirby [56] DFT calculations at the B3LYP/6-31 G (d,p) level were done in the gas phase as well as in ether and water.

Computations were directed toward elucidation of the transition and ground state structures (global minimum,

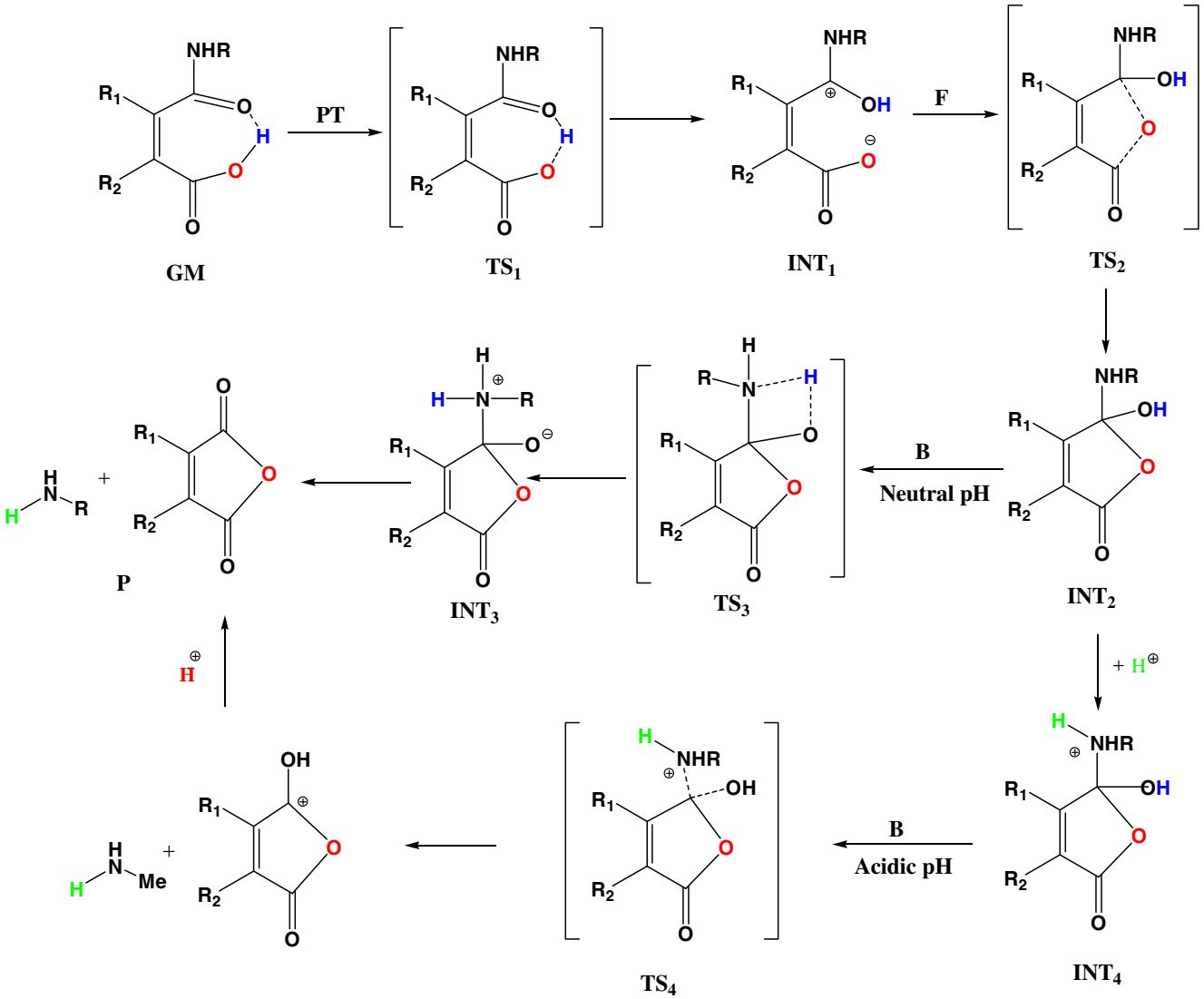

Scheme 3 Possible mechanistic routes for the acid-catalyzed hydrolysis of 1–9 and ProD 1–2. R, R1 and R2 are alkyl groups. PT, F and B refer to proton transfer, tetrahedral intermediate formation and tetrahedral intermediate breakdown, respectively. GM, INT, TS and P refer to global minimum, intermediates, transition states and products, respectively

intermediates and products) for the acid-catalyzed hydrolysis of **1**–**9** and **ProD 1**–**2** in the presence of one molecule of water, a cluster of water, in the gas phase and in ether. It is expected that the stability of the chemical entities (GM, TS and etc.) will be different in the gas phase or solvent having low dielectric constant compared to that in water (a relatively high dielectric constant).

General consideration

Because the energy of a carboxylic acid amide molecule is strongly dependent on its conformation and the latter determines its ability to be engaged in intramolecular hydrogen bonding, we were concerned with the identification of the most stable conformation (global minimum) for each of Kirby's acid amides **1**–**9** and prodrugs **ProD 1**–**2** calculated in this study. This was accomplished by 360° rotation of the carboxylic group about the bond C6-C7 (i.e., variation of the dihedral angle O1C7C6C5, Chart 1), and 360° rotation of the carbonyl amide group about the bond C4-C5 (i.e., variation of the dihedral angle O3C4C5C6) in increments of 10° and calculation of the conformational energies (see Chart 1).

In the DFT calculations for **1**–**9** and **ProD 1**–**2**, two types of conformations in particular were considered: one in which the amide carbonyl is *syn* to the carboxyl group and another in which it is *anti*. It was found that the global minimum structures for **1**–**9** and **ProD 1**–**2** all reside in the *syn* conformation (see Fig. 1a).

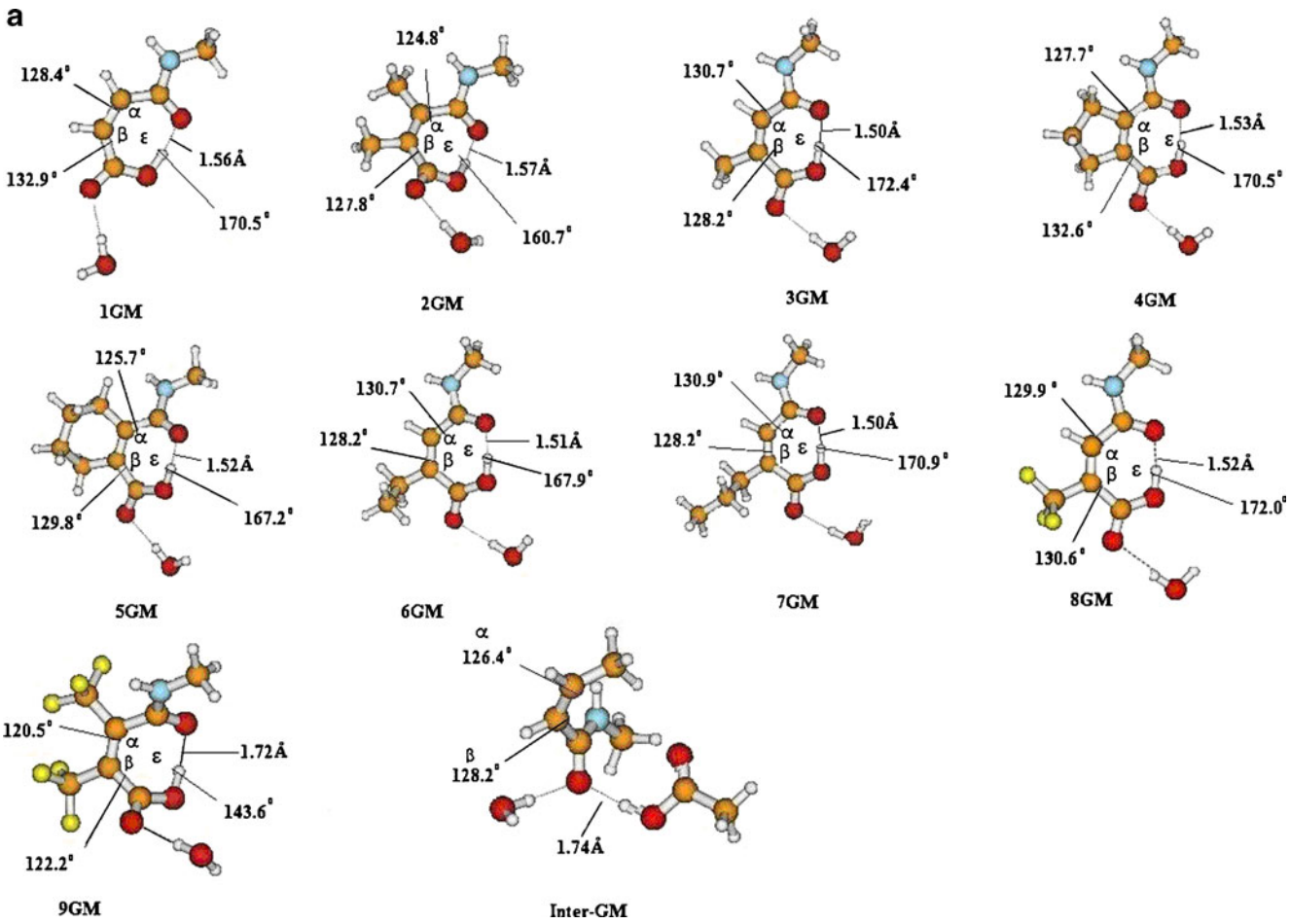

Fig. 1 (**a**) DFT optimized structures for the global minimum (GM) in processes **1**–**9** and **Inter** (**b**) DFT optimized structures for the intermediate (INT_2) in processes **1**–**9** and **Inter** (**c**) DFT optimized structures for the transition state (TS_4) in processes **1**–**9** and **Inter**

Conformational analysis for the chemical entities involved in the acid-catalyzed hydrolysis of Kirby's acid amides 1–9 and ProD 1–2

Starting geometries (GM)

Since the acid-catalyzed hydrolysis reactions of **1**–**9** were conducted in aqueous medium, we have computed the geometries of the chemical entities involved in these reactions in the presence of one molecule of water in order to account for any specific intermolecular hydrogen bonding. The calculated B3LYP/6-31 G (d,p) geometries along with selected bond distances and bond angles for the global minimum structures of **1**–**9** (**1GM-9GM**) and **ProD 1GM-2GM** are illustrated in Figs. 1a and 2, and listed in Table 1. Examination of the calculated geometries of **1GM-9GM** (Fig. 1a and Table 1) and **ProD 1GM-2GM** (Fig. 2) indicates that all of them exhibit conformation by which the carboxyl group is engaged intramolecular in a hydrogen bond with the neighboring amide oxygen. This engagement results in the formation of seven-membered ring in all the global minimum structures (see Figs. 1a and 2). The calculated B3LYP/6-31 G (d,p) intramolecular hydrogen bonding length (r_{GM} in Chart 1) in **1GM-9GM** and **ProD 1GM-2GM** was found in the range of 1.50 Å −1.87 Å and that for the hydrogen bond angle ε (the hydrogen bond angle, O1H2O3 in Chart 1) in the range of 143.6°-172.4°. Furthermore, the calculated DFT values for angles α and β were in the range of 120.5°- 130.7° and 122.2°- 133.8°, respectively. Inspection of Table 1 indicates that the calculated DFT values for the interatomic distance between the carboxyl hydroxyl oxygen and the amide carbonyl carbon range between 3.05 Å and 3.16 Å, while the angle of attack (C(O)OH/C(O)/C(O), angle θ in Chart 1) was found in the range 49.8°-56.8°.

Tetrahedral intermediate geometries (INT2)

The calculated DFT properties for the tetrahedral intermediate geometries of **1**–**9** (**1INT2-9INT2**) and **ProD 1INT_2-2INT_2** are shown in Figs. 1b and 2 and are tabulated in Table 1. Examination of the calculated structures for these

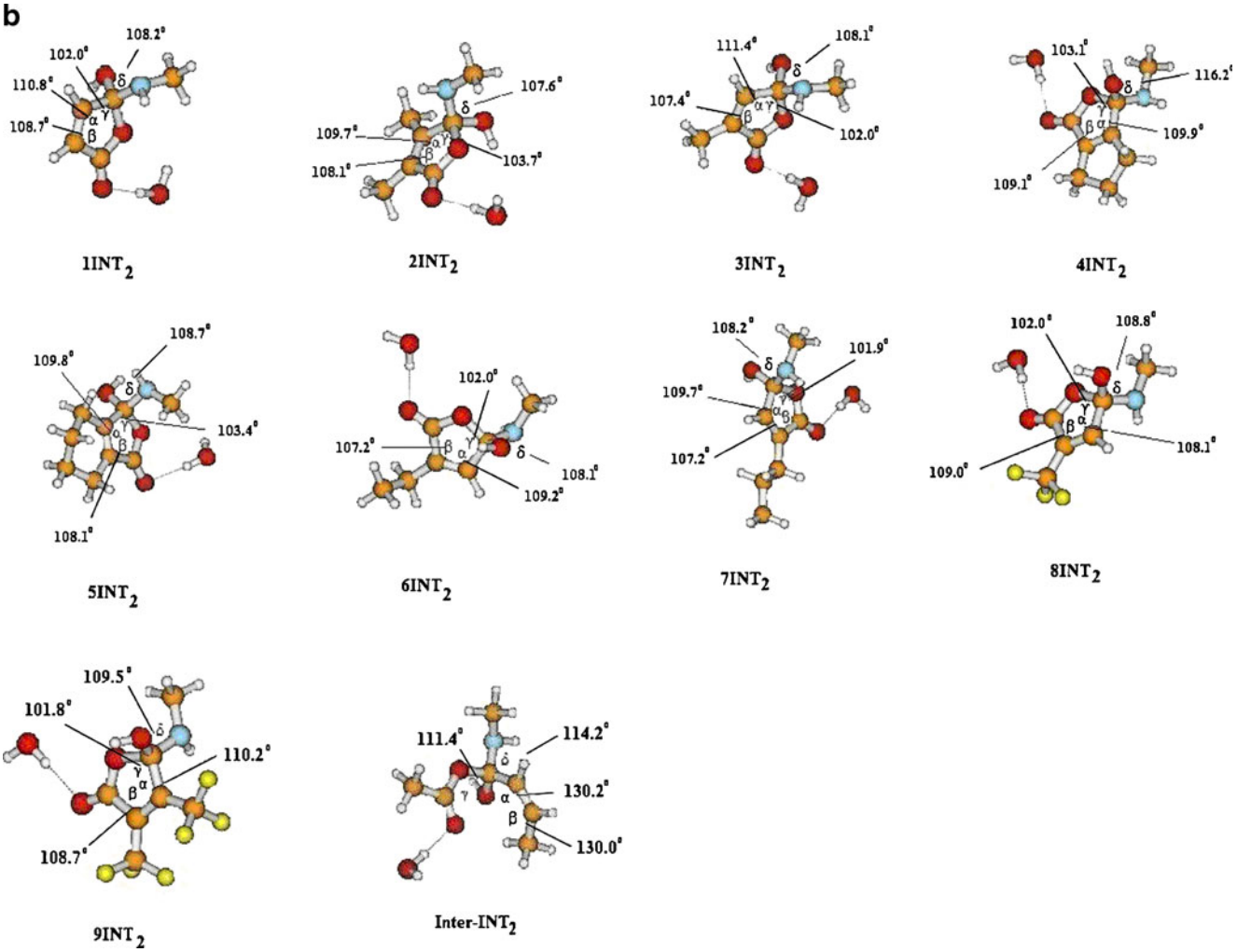

Fig. 1 continued

intermediates revealed that angles α and β values in the intermediates are reduced when compared to that in the corresponding global minimum structures. The α values range was 107.2°-109.1° whereas for β values the range was 108.1°-111.4°. Furthermore, the angles γ and δ were in the range for similar regular tetrahedral intermediates. The range for γ was 102.0°- 103.7° and for δ was 107.6°- 116.2°.

Transition state geometries for the tetrahedral intermediate dissociation (TS4)

The calculated properties for the transition state geometries of the tetrahedral intermediate collapse in **1**–**9** and **ProD 1**–**2** (**1TS$_4$-9TS$_4$**, **ProD 1TS$_4$** and **ProD 2TS$_4$**) are summarized in Table 1 and illustrated in Figs. 1c and 2. Inspection of the optimized structures revealed that the geometries of the transition states resemble that of the corresponding tetrahedral intermediates. The angle α and β values are quite identical in both the tetrahedral intermediates and their corresponding transition states. The range of the α values were found in the range 107.0°-108.4° and that of β was in the range 108.3°-109.2°.

Mechanistic investigation

Using the quantum chemical package Gaussian-98 [58] we calculated the DFT at B3LYP/6-31 G (d,p) level of theory kinetic and thermodynamic properties for all possible routes for the acid-catalyzed reactions of Kirby's acid amides **1**–**9** and **ProD 1**–**2**. The proposed routes are illustrated in Scheme 3.

The enthalpy and entropy energy values in the gas phase, ether and in the presence of a cluster of water for the global minimum structure (GM), the products (P) and the corresponding transition states, TS_1, TS_2, TS_3 and TS_4, and corresponding intermediates INT_1, INT_2, INT_3 and INT_4 for the suggested routes in the acid-catalyzed hydrolysis of **1**–**9** and **ProD 1**–**2** were calculated

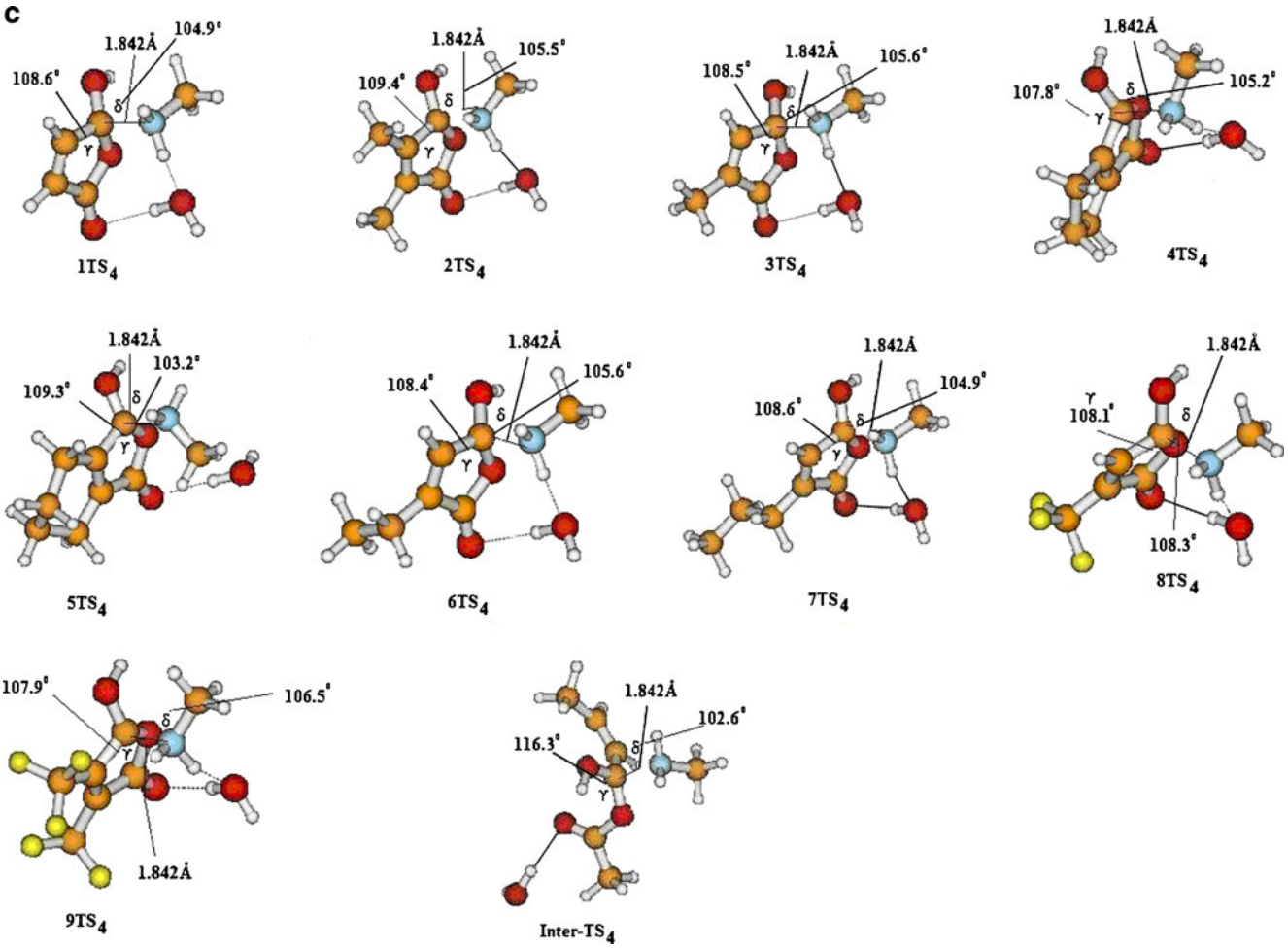

Fig. 1 continued

(Scheme 3). Table 2 lists the energy values for **1GM-9GM**, **ProD 1GM**, **ProD 2GM**, **1INT$_2$-9INT$_2$**, **ProD 1INT$_2$**, **ProD 2INT$_2$**, **1TS$_4$-9TS$_4$**, **ProD 1TS$_4$** and **ProD 2TS$_4$**. Figs. 1a, b, c and 2 depict the DFT optimized structures for GM, INT$_2$ and TS$_4$ in **1**–**9** and **ProD 1**–**2**.

Using the calculated DFT values for the enthalpy and entropy of the GM and the four transition states in the hydrolysis of **1**–**9** and **ProD 1**–**2** the enthalpy activation energies ($\Delta H^{\ddagger}$), entropy activation energies ($T\Delta S^{\ddagger}$), and the free activation energies in the gas phase, ether and water ($\Delta G^{\ddagger}$) for the various routes in the mentioned processes (Scheme 3) were calculated and are summarized in Tables 3 and 4.

Inspection of the calculated B3LYP/6-31 G (d,p) activation energy values listed in Tables 3 and 4 revealed that the rate-limiting step for the acid-catalyzed hydrolysis of **1**–**9** and **ProD 1**–**2** is dependent on the medium by which the calculations were done. When the calculations were run in the gas phase the formation of the tetrahedral intermediate, step F in Scheme 3, was the rate limiting step, whereas when the calculations were executed in the presence of a cluster of water the step by which the tetrahedral intermediate breaks down was the rate-limiting (step B in Scheme 3). On the other hand, the energy calculations in the presence of ether indicate that while in some processes such as **2**, **5** and **ProD 2** the rate-limiting step is the one by which the carboxyl group approaches the amide carbonyl carbon to form the tetrahedral intermediate (step F in Scheme 3) the rate in processes **1**, **3**–**4**, **6**–**9** and **ProD 1** is determined on the step by which the tetrahedral intermediate collapses to yield products (step B in Scheme 3).

The gas phase energy barrier for the proton transfer process (step PT in Scheme 3), tetrahedral intermediate formation (F) and tetrahedral intermediate breakdown (step B in Scheme 3) were found in the range 17.77-19.33 kcal mol^{-1}, 25.94-45.37 kcal mol^{-1} and 15.25-36.77 kcal mol^{-1}, respectively (Table 3). Furthermore, the gas phase free activation energy for the rate-limiting step (F) is about 5–15 kcal higher than that for the breakdown process. On the other hand, the activation energies difference as calculated in water between the

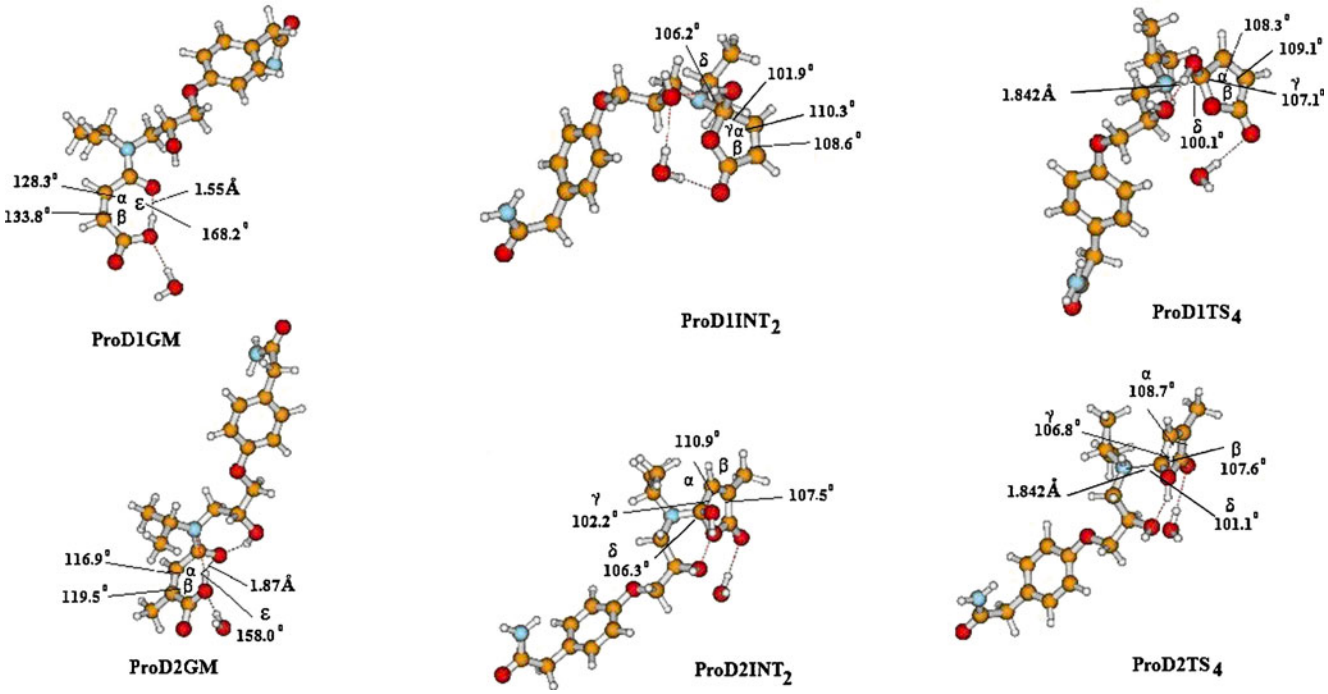

Fig. 2 DFT optimized structures for the global minimum (GM), intermediate (INT_2) and transition state (TS_4) in processes **ProD 1–2**

intermediate collapse and intermediate formation, is about 2–9 kcal mol^{-1} (Table 4).

The factors affecting the hydrolysis rate

Careful inspection of Tables 3 and 4 revealed that both the substituent on the double bond and the reaction medium has a profound effect on the reaction rate.

1. **The substituent effect**: to examine the structural factors associated with high reactivity such as in systems **2**, **5** and **ProD 2**, analysis of the conformation of the rigid structures of the ground states should be evaluated. A careful examination of Tables 1 and 4 revealed the existence of two significant trends in the reactivity versus the structural features of the ground state structures. The closest distance of approach of the carboxyl oxygen and the amide oxygen in the ground state (r_{AP} in Chart 1) is less for more reactive compounds. For example, the distance for the unsubstituted maleamic acid amide **1** is 3.16 Å whereas for the dimethylsubstituted derivative **2** is 3.05 Å. In fact,

Table 1 DFT (B3LYP) calculated geometries for GM, INT_2 and TS_4 in **1–9** and **ProD 1-2**

System	α in GM	β in GM	α in INT_2	β in INT_2	γ in INT_2	δ in INT_2	α in TS_4	β in TS_4	γ in TS_4	δ in TS_4	θ in GM	r_{AP} in GM
1	128.4	132.9	108.7	110.8	102.0	108.2	107.6	108.5	108.6	104.9	50.3	3.16
2	124.8	127.8	108.1	109.7	103.7	107.6	107.0	108.3	109.4	105.5	53.0	3.05
3	130.7	128.2	107.4	111.4	102.0	108.1	107.3	108.7	108.5	105.6	51.0	3.10
4	127.7	132.6	109.1	109.9	103.1	116.2	108.2	109.8	107.8	105.2	49.8	3.15
5	125.7	129.8	108.1	109.8	103.4	108.7	107.2	108.8	109.3	103.2	51.6	3.09
6	130.7	128.2	107.2	109.2	102.0	108.1	107.1	108.8	108.4	105.6	51.4	3.09
7	130.9	128.2	107.2	109.7	101.9	108.2	107.2	108.8	108.6	104.9	51.1	3.09
8	129.9	130.6	109.0	108.1	102.0	108.8	107.6	109.2	108.1	108.3	51.0	3.11
9	120.5	122.2	108.7	110.2	101.8	109.5	107.6	108.6	107.9	106.5	56.8	3.05
ProD 1	128.3	133.4	108.8	110.3	101.9	115.6	108.4	108.7	107.1	106.3	48.7	3.19
ProD 2	126.2	129.6	107.5	110.9	102.2	115.2	107.6	108.7	106.8	103.0	55.1	3.32

B3LYP refers to values calculated by B3LYP/6-31 G (d, p) method. GM, INT_2 and TS_4 refer to global minimum, intermediate and transition state structures, respectively (see Scheme 3). For the definition of the bond angles α, β, γ and δ see Fig. 1a, b and c. For the definition of rAP see Chart 1.The angle unit is degree and the r_{AP} unit is Å

Table 2 DFT (B3LYP/6-31 G (d,p)) calculated properties for the acid catalyzed hydrolysis of acid amides **1**–**9**, **ProD 1**–**2** and **Inter**

Compound	Enthalpy, H (gas phase) In Hartree	(gas phase) Entropy, S, Cal/Mol-Kelvin	Frequency Cm^{-1}	MM2Es kcal/mol
1GM	−551.6209552	115.71	———	10.16
$1INT_2$	−551.5899873	113.12	———	20.55
$1TS_4$	−551.9510979	100.58	29.18i	———
2GM	−630.2556684	133.45	———	10.82
$2INT_2$	−630.2424070	125.08	———	16.16
$2TS_4$	−630.6125865	117.89	57.26i	———
3GM	−590.9452364	126.16	———	9.40
$3INT_2$	−590.9162845	124.52	———	17.32
$3TS_4$	−591.284155	109.50	45.91i	———
4GM	−668.3716758	131.90	———	12.30
$4INT_2$	−668.3272626	125.09	———	27.89
$4TS_4$	−668.7001822	116.95	73.72i	———
5GM	−707.6805570	136.69	———	9.18
$5INT_2$	−707.6689275	122.73	———	19.25
$5TS_4$	−707.6321442	122.88	118.05i	———
6GM	−630.2606708	132.74	———	5.12
$6INT_2$	−630.2326178	132.45	———	17.59
$6TS_4$	−630.60156591	116.93	52.77i	———
7GM	−669.5780833	138.31	———	6.20
$7INT_2$	−669.5495044	137.75	———	18.55
$7TS_4$	−669.9185072	124.96	68.64i	———
8GM	−888.6478787	140.60	———	12.86
$8INT_2$	−888.6201859	137.62	———	22.34
$8TS_4$	−888.9742696	120.84	37.75i	———
9GM	−1225.6575172	145.62	———	28.29
$9INT_2$	−1225.6422023	147.77	———	26.92
$9TS_4$	−1225.9938255	140.05	33.82i	———
ProD 1GM	−1337.6974501	214.38	———	20.97
ProD $1INT_2$	−1337.6654432	188.26	———	41.97
ProD $1TS_4$	−1338.0399174	158.59	70.33i	———
ProD 2GM	−1377.0175828	210.68	———	17.31
ProD $2INT_2$	−1376.9882479	211.30	———	38.42
ProD $2TS_4$	−1377.3516015	193.30	123.35i	———
InterGM	−631.4579281	141.61	———	2.98
$InterINT_2$	−631.4282861	129.50	———	13.64
$InterTS_4$	−631.7933134	130.70	57.27i	———

GM, INT and TS are global minimum, intermediate and transition state structures, respectively. MM2Es is the strain energy calculated by Allinger's MM2 method [67]

when the values of r_{AP} were examined for correlation with the experimental and water calculated free activation energies ($\Delta G_B^{\ddagger}$) strong correlations with correlation coefficient of R=0.92 -0.96 were obtained (Fig. 3a). The second structural factor that might have a significant effect on the reactivity of an acid amide is the angle by which the carboxyl group approaches the amide carbonyl carbon (the attack angle ρ, see Chart 1). The calculated θ values for the reactive derivatives were found to be larger than those for the less reactive acid amides. For example the calculated θ value for system **2** was 53° whereas for **4** was 49.8°. Linear correlation with strong correlation coefficients (R= 0.92-0.96) were found between the DFT calculated ρ values and the experimental and water calculated free activation energy values (Fig. 3b) to shed some light on the factors responsible for the unusual accelerations in rate and to examine whether the discrepancy in rates for processes **1**–**9** stems from steric effects (strain energy) or other effects we have calculated, using Allinger's MM2 method [67], the strain energy values for the reactants (GM), intermediates (INT) and products (P) in **1**–**9** and **ProD 1**–**2**. The MM2 strain energies (Es) for these geometries are listed in Table 4. The MM2

Table 3 DFT (B3LYP) calculated kinetic and thermodynamic properties in the gas phase for the acid catalyzed hydrolysis of **1**–**9**, **ProD 1**–**2** and **Inter**

System	$\Delta H_{BGP}^{\ddagger}$ (kcal/mol)	$T\Delta S_{BGP}^{\ddagger}$ (kcal/mol)	$\Delta G_{BGP}^{\ddagger}$ (kcal/mol)	$\Delta H_{FGP}^{\ddagger}$ (kcal/mol)	$T\Delta S_{FGP}^{\ddagger}$ (kcal/mol)	$\Delta G_{FGP}^{\ddagger}$ (kcal/mol)	$\Delta G_{BEth}^{\ddagger}$ (kcal/mol)	$\Delta G_{FEth}^{\ddagger}$ (kcal/mol)	$\Delta G_{BGP}^{\ddagger}$ (kcal/mol) In high pH
1	27.31	−0.77	28.08	32.46	−1.09	33.53	34.27	31.35	45.55
2	13.93	−2.49	16.42	25.67	−1.41	27.08	16.32	21.29	33.59
3	24.41	−0.49	24.90	30.68	−1.89	32.57	29.53	28.23	44.68
4	34.42	−2.35	36.77	41.88	−3.49	45.37	40.23	39.27	53.5
5	13.25	−4.16	17.41	24.55	−2.32	26.87	18.51	22.34	34.52
6	23.83	−0.09	23.92	30.11	−2.01	32.12	29.53	27.50	45.72
7	24.86	−0.17	25.03	30.76	−1.54	32.30	28.35	27.76	———
8	24.08	−0.89	24.87	29.79	−2.58	32.37	29.76	28.20	———
9	17.88	0.64	17.24	24.17	−1.77	25.94	24.46	18.69	———
ProD 1	20.08	−7.78	27.86	29.96	−5.99	35.95	38.76	39.49	———
ProD 2	15.43	0.18	15.25	31.94	1.19	30.75	21.15	24.35	43.53
Inter	39.90	−3.35	43.25	———	———	———	———	———	———

B3LYP refers to values calculated by B3LYP/6-31 G (d, p) method. $\Delta H^{\ddagger}$ is the calculated activation enthalpic energy (kcal/mol). $T\Delta S^{\ddagger}$ is the calculated activation entropic energy (kcal/mol). $\Delta G^{\ddagger}$ is the calculated activation free energy (kcal/mol). B and F refer to tetrahedral intermediate breakdown and tetrahedral intermediate formation. GP and Eth refer to calculated in the gas phase and in ether, respectively

calculated Es values were examined for correlation with the experimental relative rate values, log k_{rel} (Table 4). Strong correlations were obtained with a correlation coefficient R=0.94 for the correlation with the intermediates values and R=0.97 for the values of the products (Fig. 3c). Furthermore, good correlations were obtained between the experimental and calculated free activation energy values on one hand and the strain energy difference values between the intermediates and reactants (Es_{INT-GM}) on the other hand (R=0.85-0.94) (Fig. 3d). The results shown in Fig. 3c and d indicate that the rate of the reaction for systems having less-strained intermediates or products such as **2** and **5** are higher than that having more strained intermediates or products such as **1** and **4**. This might be attributed to the fact that the transition state structures in **1**–**9** resemble that of the corresponding intermediates or products (Figs. 2b and c).

In order to test whether the substituent on the double bond has the same effect on the tetrahedral intermediate

Table 4 DFT (B3LYP) calculated kinetic and thermodynamic properties for the acid catalyzed hydrolysis of **1**–**9**, **ProD 1**–**2** and **Inter**

System	$\Delta H_{BW}^{\ddagger}$ (kcal/mol)	$\Delta G_{BW}^{\ddagger}$ (kcal/mol)	log k_{rel} [56]	log EM (Exp) [56]	log EM (Calc)	Es (INT_2) (kcal/mol)	Es (P) (kcal/mol)	Es (GM) (kcal/mol)	$\Delta G_{FW}^{\ddagger}$ (kcal/mol)	Exp $\Delta G^{\ddagger}$ [12](kcal/mol)
1	32.29	33.06	0	7.724	8.52	20.55	25.08	10.16	26.10	23.70
2	17.56	20.05	4.371	15.86	18.08	16.16	18.93	10.82	17.90	17.30
3	27.93	28.42	1.494	7.742	11.93	17.32	21.70	9.40	24.80	21.14
4	35.76	38.11	−4.377	1.255	4.81	27.89	32.75	12.30	32.16	30.70
5	18.96	23.12	2.732	15.190	15.82	19.25	23.13	9.18	17.89	19.75
6	27.19	27.28	1.516	6.962	12.76	17.59	22.95	5.12	23.87	———
7	27.38	27.55	1.648	8.568	12.57	18.55	24.00	6.20	24.40	———
8	29.23	30.12	———	———	6.36	22.34	27.77	12.86	23.66	
9	15.79	15.15	———	———	21.68	26.92	35.64	28.29	11.97	
ProD 1	31.37	39.12	———	———	4.06	41.97	25.08	20.97	35.76	
ProD 2	26.98	26.8	———	———	13.11	38.42	18.98	17.31	17.85	
Inter	41.30	44.65	———	———	———	13.64	12.10	———	———	———

B3LYP refers to values calculated by B3LYP/6-31 G (d, p) method. $\Delta H^{\ddagger}$ is the calculated activation enthalpic energy (kcal/mol). $T\Delta S^{\ddagger}$ is the calculated activation entropic energy (kcal/mol). $\Delta G^{\ddagger}$ is the calculated activation free energy (kcal/mol). Es refers to strain energy calculated by Allinger's MM2 method [67]. INT_2 and P refer to intermediate two and product, respectively. EM=$e^{-(\Delta G^{\ddagger}inter - \Delta G^{\ddagger}intra)/RT}$. BW and FW refer to tetrahedral intermediate breakdown and tetrahedral intermediate formation calculated in water, respectively. Exp refers to experimental value. Calc refers to DFT calculated values

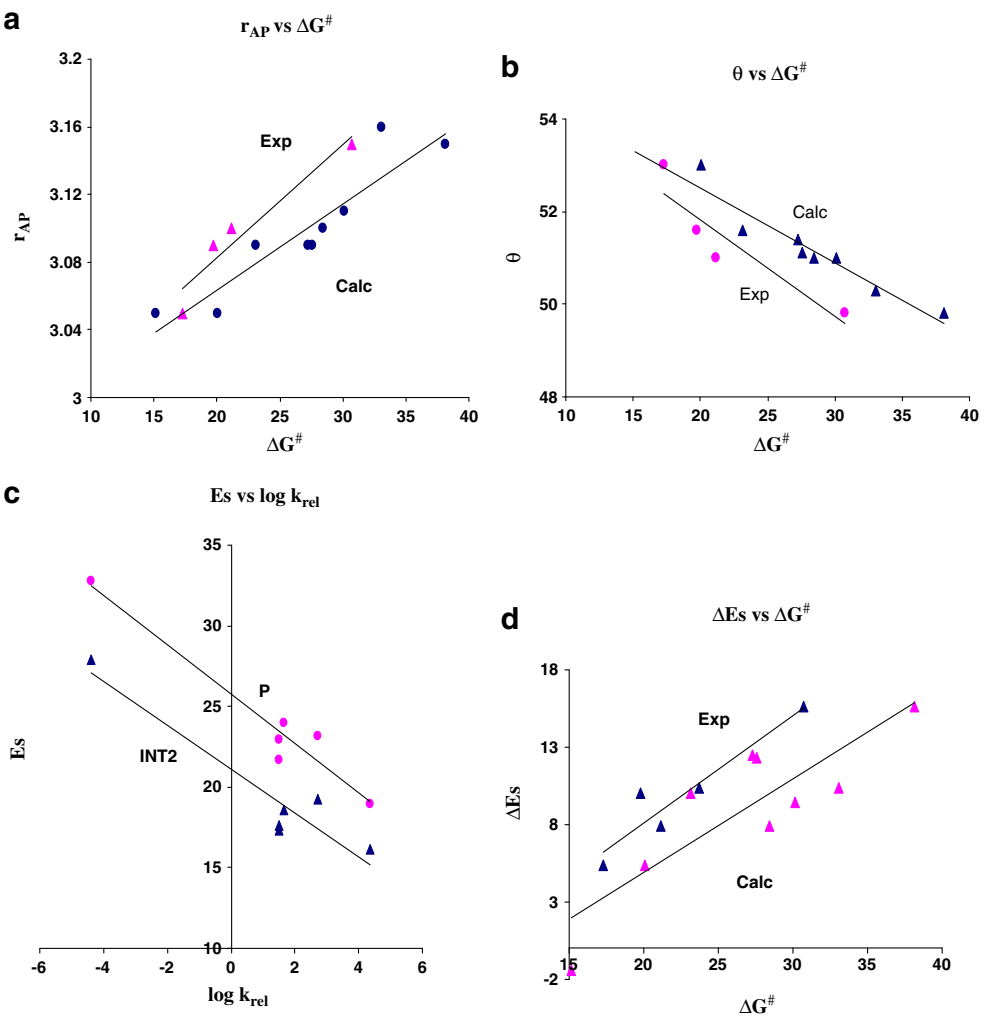

Fig. 3 (**a**) Plot of r_{AP} vs. $\Delta G^{\ddagger}$ in **1**–**9**, where the blue points for the DFT calculated values (in water) and the pink points for the experimental values. r_{AP} is the distance between the hydroxyl oxygen of the carboxylic group and the carbon of the amide carbonyl in the reactant. $\Delta G^{\ddagger}$ is the free activation energy. (**b**) Plot of ρ vs. $\Delta G^{\ddagger}$ in **1**–**9**, where the blue points for the DFT calculated values (in water) and the pink points for the experimental values. ρ is the angle of attach of the approach of the hydroxyl of the carboxylic group toward the carbon of the amide carbonyl in the reactant. $\Delta G^{\ddagger}$ is the free activation energy. (**c**) Plot of Es vs. log k_{rel} in **1**–**9**, where the blue points for the intermediates (INT2, see Scheme 3) and the pink points for the products (P, see Scheme 3). log k_{rel} is the relative rate. (**d**) Plot of ΔEs vs. $\Delta G^{\ddagger}$ in **1**–**9**, where the blue points for the experimental values and the pink points for the DFT calculated values (in water). $\Delta G^{\ddagger}$ is the free activation energy

formation (step F in Scheme 3) and the tetrahedral intermediate collapse (B in Scheme 3), the DFT calculated activation energies in the gas phase and in water for the formation of the tetrahedral intermediate ($\Delta G_F^{\ddagger}$) were correlated with the energy values needed for its collapse ($\Delta G_B^{\ddagger}$). The correlation results illustrated in Fig. 4a indicate strong correlations with a correlation coefficient R=0.92 and 0.95, respectively. This indicates that the driving force for the formation and collapse of the tetrahedral intermediate is the same and the rate of the hydrolysis reaction is dependent on strain effects.

The combined results might be able to test some theories that were invoked to account for rate accelerations in intramolecular and enzymatic processes. Such theories are the orbital steering theory of Koshland [68] that describes the effect of critical angle of approach on reactivity, and Bruice's [31, 32] and Menger's proximity orientation [36–43].

2. **The solvent effect**: Inspection of Scheme 3 revealed that the step in the intramolecular hydrolysis reaction most powerfully affected by structural changes and solvent effects are the ring-closure of INT_1 which is involved in the tetrahedral intermediate formation. Examination of the geometries of the corresponding transition states for INT_2 (TS_2) indicates that TS_2 is in the ionic form. It is expected that the effect of polar solvents on the stability of TS_2 will be different from those with less polarity. The free activation energies for the approach process ($\Delta G_F^{\ddagger}$) and the dissociation process ($\Delta G_B^{\ddagger}$) calculated in the gas phase, ether and in presence of a cluster of water listed in Tables 3 and 4 indicate that solvents with low dielectric constant such in the case of the gas phase tend to shift the equilibrium to the side of the reactants by destabilizing TS_2 and thus making the approach step as the rate-limiting whereas solvents with high dielectric constants such as water interact strongly with the ionic transition state. These interactions stabilize the approach transition state (TS_2) and consequently lower the approach barrier, hence making the reaction rate dependent on the dissociation step. A representation of the energy profiles

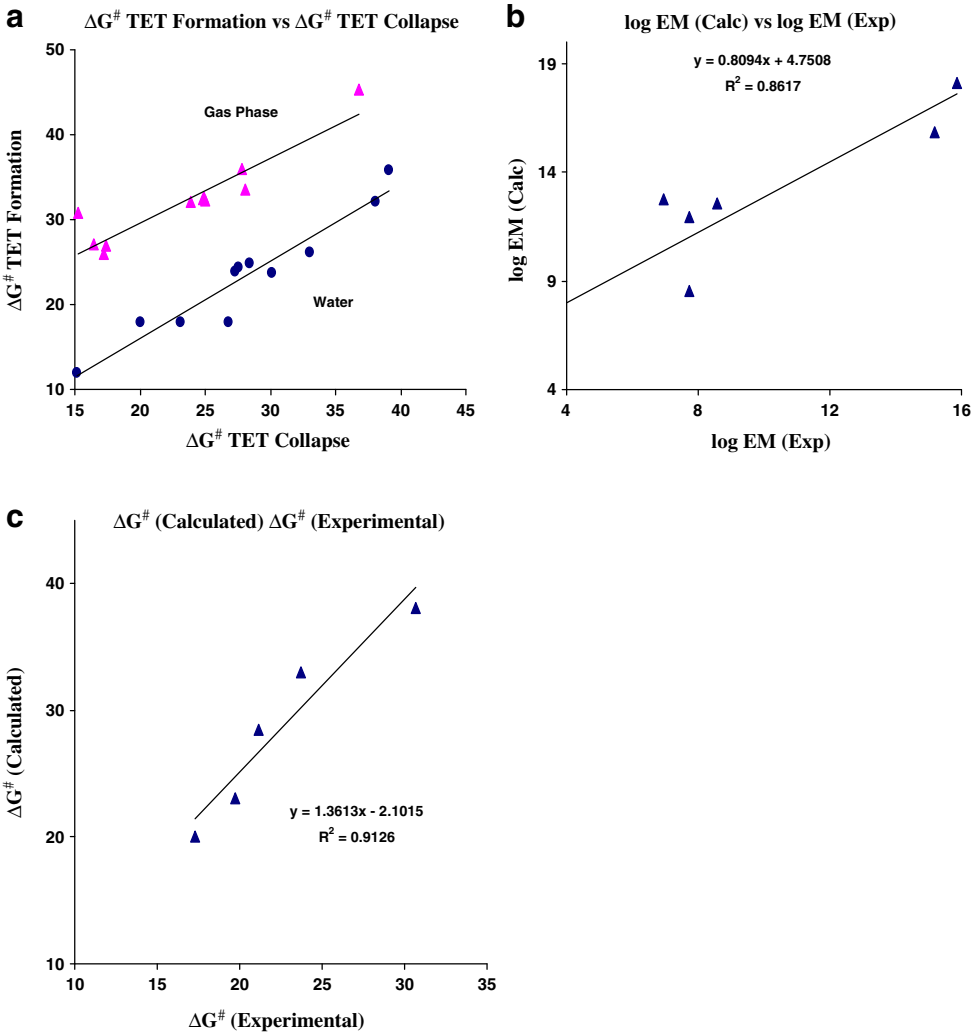

Fig. 4 (**a**) Plot of $\Delta G^{\ddagger}$ (Formation) vs. $\Delta G^{\ddagger}$ (Collapse) in **1**–**9**, where the blue points for the DFT calculated values (in water) and the pink points for that calculated in the gas phase. $\Delta G^{\ddagger}$ (Formation) and $\Delta G^{\ddagger}$ (Collapse) are the free activation energy needed for the tetrahedral intermediate formation and collapse, respectively. (**b**) log EM (Calc) vs. log EM (Exp) in **1**–**9**. EM refers to effective molarity. Calc and Exp refer to calculated by DFT and experimental, respectively. (**c**) Plot of $\Delta G^{\ddagger}$ (Calculated) vs. $\Delta G^{\ddagger}$ (Experimental) in **1**–**9**. $\Delta G^{\ddagger}$ (Calculated) and $\Delta G^{\ddagger}$ (Experimental) are the DFT calculated (in water) free activation energy and experimental free activation energy, respectively

for the hydrolysis of **ProD 1** as calculated in the gas phase and in presence of a cluster of water is illustrated in Fig. 5.

On the other hand, the DFT calculations in presence of ether having dielectric constant of 4.5 indicate that in systems **2, 5** and **ProD 1–2** the rate-limiting step is the formation of the tetrahedral intermediate whereas in the other processes the rate-limiting step is the dissociation of the tetrahedral intermediate (see Tables 3 and 4).

Calculations of the effective molarity (EM) values for processes 1–9 and ProD 1–2

It is widely accepted that the measure for intramolecular efficiency is the effective molarity (EM). The effective molarity is defined as a ratio of the intramolecular rate and its corresponding intermolecular where both processes are driven by identical mechanisms. Ring size, solvent and reaction type are the main factors affecting the EM parameter. Ring-closing reactions via intramolecular nucleophilic addition are much more efficient than intramolecular proton transfers. Values in the order of 10^{9}-10^{13} M have been measured for the EM in intramolecular processes occurring through nucleophilic addition. Whereas for proton transfer processes EM values of less than 10 M were obtained [69].

To obtain credibility for our calculation results we introduce our computation rational for calculating the EM values for processes **1**–**9** and **ProD 1–2** based on the DFT calculated activation energies ($\Delta G^{\ddagger}$) of **1**–**9** and **ProD 1–2**, and the corresponding intermolecular process **Inter** (Scheme 2).

The intermolecular process **Inter** (Scheme 2) was calculated to be used in the calculation of the effective molarity values (EM) for the corresponding intramolecular processes **1**–**9** and **ProD 1–2**.

Utilizing Eqs. 1–4, we derived Eq. 5 which describes the EM parameter as a function of the difference in the

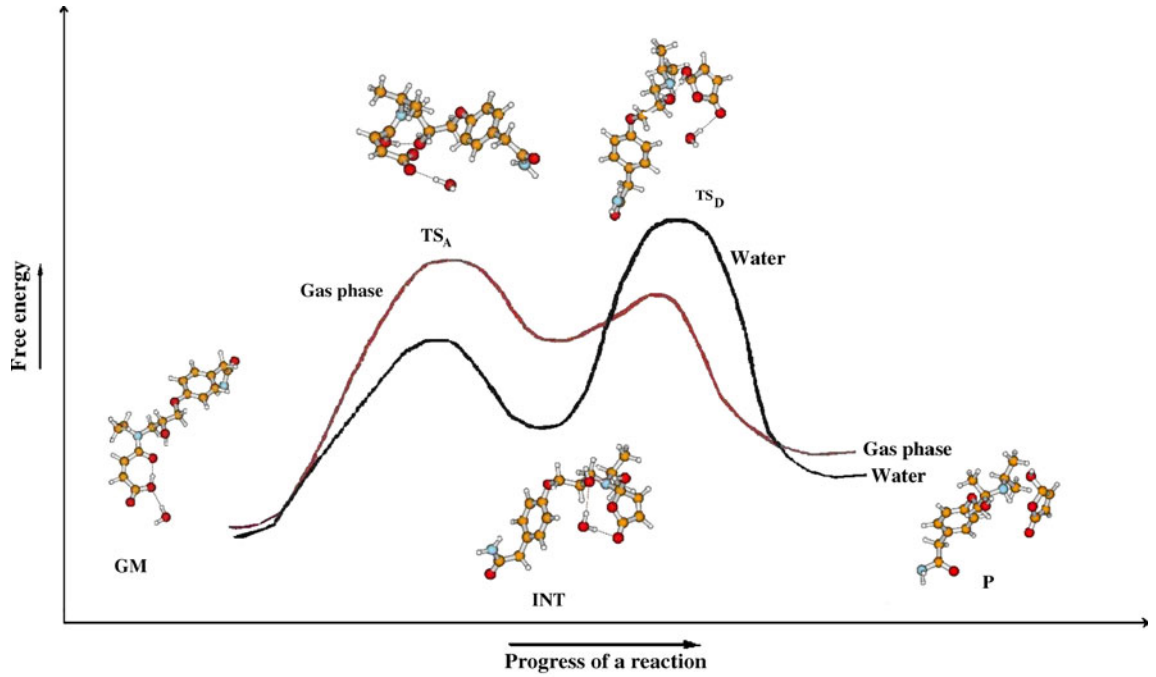

Fig. 5 A representation of an energy profile for acid-catalyzed hydrolysis of ProD 1 as calculated in the gas phase (GP) and in water (W). GM. TS, INT and P refer to global minimum, transition state, intermediate and product structures, respectively. TS_A and TS_D are approach and dissociation transition state structures, respectively

activation energies of the intra- and the corresponding intermolecular processes. Table 4 lists the calculated EM values for processes **1**–**9** and **ProD 1–2** as calculated by Eq. 5,

$$EM = k_{intra}/k_{inter} \quad (1)$$

$$\Delta G^{\ddagger}_{inter} = -RT \ln k_{inter} \quad (2)$$

$$\Delta G^{\ddagger}_{intra} = -RT \ln k_{intra} \quad (3)$$

$$\Delta G^{\ddagger}_{intra} - \Delta G^{\ddagger}_{inter} = -RT \ln k_{intra}/k_{inter} \quad (4)$$

$$\ln EM = -\left(\Delta G^{\ddagger}_{intra} - \Delta G^{\ddagger}_{inter}\right)/RT \quad (5)$$

where T is the temperature in Kelvin and R is the gas constant.

The calculated log EM values listed in Table 4 were examined for correlation with the corresponding log EM experimental values [56]. The correlation results along with the correlation coefficients are illustrated in Fig. 4b. Inspection of the log EM values listed in Table 4 and Fig. 4b revealed that **2** and **5** were the most efficient processes among **1**–**9**, whereas process **4** was the least. The discrepancy in rates between **2** and **5** on one hand and **4** on the other hand is attributed to strain effects.

Although the calculated and experimental EM values are comparable there is a discrepancy in their absolute values. This is due to the fact that the experimental measurement of the EM values in **1**–**9** was conducted in the presence of aqueous acid whereas the DFT calculations were done in plain water. The dielectric constant value for a mixture of acid/water is expected to be different from that of water (78.39) and hence the discrepancy in the calculated and experimental EM values [70].

In order to draw more credibility to our DFT calculations the calculated DFT free activation energies in water ($\Delta G_{BW}^{\ddagger}$) were correlated with the corresponding experimental free activation energies (Exp $\Delta G^{\ddagger}$) [56]. Strong correlations were found with R value of 0.96 (Fig. 4c).

Calculation of the $t_{1/2}$ values for the cleavage reactions of prodrugs ProD 1–2

The calculated DFT properties for processes **ProD 1–2** including the geometries of global minimum (GM), intermediate (INT2) and transition state (TS4) structures are shown in Fig. 2 and listed in Tables 1, 2, 3, 4. Comparison of these structures to that calculated for processes **1**–**9** revealed a close similarity.

Using Eq. 6 obtained from the correlation of log k_{rel} vs. $\Delta G^{\ddagger}$ (Fig. 4d) and the $t_{1/2}$ value for process 2 ($t_{1/2}$=1 second) [56], we have calculated the $t_{1/2}$ values for **ProD**

1 and **ProD 2**. The calculated $t_{1/2}$ at pH 2 for **ProD 1** and **ProD 2** are 65.3 hours and 11.8 minutes, respectively.

$$\log k_{rel} = -0.4421\Delta G^{\ddagger} + 13.534 \quad (6)$$

Conclusions and future directions

The DFT calculations confirmed that the acid-catalyzed hydrolysis mechanism in Kirby's acid amides **1**–**9** involves: (1) a proton transfer from the hydroxyl of the carboxyl group to the adjacent amide carbonyl carbon, (2) an approach of the carboxylate anion toward the protonated amide carbonyl carbon to form tetrahedral intermediate; and (3) collapse of the tetrahedral intermediate into products. Furthermore, DFT calculations in different media revealed that the reaction rate-limiting step depends on the reaction medium. In aqueous medium the rate-limiting step is a collapse of the tetrahedral intermediate whereas in the gas phase the formation of the tetrahedral intermediate is the rate-limiting step. Furthermore, the calculations establish that the acid-catalyzed hydrolysis efficiency is largely sensitive to the pattern of substitution on the carbon-carbon double bond. The hydrolysis rate was found to be linearly correlated with the following: (a) the strain energy of the tetrahedral intermediate and product and the strain energy difference between the intermediate and the reactant. (b) The distance between the hydroxyl oxygen of the carboxyl group and the amide carbonyl carbon, and (c) the attack angle by which the approach step commences. Further, a linear correlation between the calculated DFT EM values and the experimental EM values demonstrates the credibility of using DFT methods in predicting energies as well as rates for reactions of the type described herein.

Utilizing the linear correlation of the experimental log k_{rel} and EM values the predicted $t_{1/2}$ values of proposed two atenolol prodrugs, **ProD 1**–**2** were predicted.

The strategy to achieve desirable prodrugs of atenolol that are capable of being stable in aqueous solutions and to have the potential for releasing atenolol in a slow release manner is: (1) synthesis of the linker and coupling of the parent drug to the linker using Kirby's synthetic procedure [36]; (2) kinetic studies (in vitro) of the synthesized prodrugs (**ProD 1**–**2**) will be performed in physiological environment (37 °C, pH =2.0 and 6.0 in aqueous medium) and (3) for the prodrugs that show desirable aqueous stability and slow release in the in vitro studies, in vivo pharmacokinetic studies will be conducted in order to determine the bioavailability and the duration of action of the tested prodrugs. In the light of the in vivo pharmacokinetics new prodrugs will be designed and synthesized.

Acknowledgments The Karaman Co. is thanked for support of our computational facilities. Special thanks are also given to Angi Karaman, Donia Karaman, Rowan Karaman and Nardene Karaman for technical assistance.

References

1. Foppa T, Murakami FS, Silva MA (2007) Development, validation and stability study of pediatric atenolol syrup. Pharmazie 62:519–521
2. Anroop B, Ghosh B, Parcha V, Khanam J (2009) Transdermal delivery of atenolol: effect of prodrugs and iontophoresis. Curr Drug Delivery 6:280–290
3. Mcainsh J, Simpson WT, Holmes BF, Young J, Ellis SH (1980) Bioavailability of atenolol formulations. Biopharm Drug Dispos 1:223–232
4. Vergin H, Nitsche V (1989) Oral bioavailability of atenolol. J Int Med Res 17:417–425
5. Shin SC, Choi JS (2003) Enhanced bioavailability of atenolol by transdermal administration of the ethylene-vinyl acetate matrix in rabbits. Eur J Pharm Biopharm 56:439–443
6. http://en.wikipedia.org/wiki/atenolol
7. http://homepage.ntlworld.com/bhandari/Imperial/Atenolol/Synthesis.htm
8. Chan K, Swenden J (2007) Pilot study of the short-term physico-chemical stability of atenolol tablets stored in a multi-compartment compliance aid. Eur J Hosp Pharm Sci 13:60–66
9. Testa B, Mayer J (2003) Hydrolysis in drug and prodrug metabolism-Chemistry Biochemistry and Enzymology. Wiley-VHCA, Zürich
10. Testa B, Mayer JM (2001) Concepts in prodrug design to overcome pharmacokinetic problems. In: Testa B, van de Waterbeemd H, Folkers G, Guy R (eds) Pharmacokinetic optimization in drug research: biological, physiochemical and computational strategies. Wiley-VHCA, Zurich, pp 85–95
11. Wang W, Jiang J, Ballard CE, Wang B (1999) Prodrug approaches in the improved delivery of peptide drugs. Curr Pharm Des 5:265–287
12. Karaman R (2008) Analysis of Menger's spatiotemporal hypothesis. Tetrahedron Lett 49:5998–6002
13. Karaman R (2009) A new mathematical equation relating activation energy to bond angle and distance: a key for understanding the role of acceleration in the lactonization of the trimethyl lock system. Bioorg Chem 37:11–25
14. Karaman R (2009) Reevaluation of Bruice's proximity orientation. Tetrahedron Lett 50:452–456
15. Karaman R (2009) Accelerations in the lactonization of trimethyl lock systems is due to proximity orientation and not to strain effects. Res Lett Org Chem. doi:10.1155/2009/240253
16. Karaman R (2009) The effective molarity (EM) puzzle in proton transfer reactions. Bioorg Chem 37:106–110
17. Karaman R (2009) Cleavage of Menger's aliphatic amide: a model for peptidase enzyme solely explained by proximity orientation in intramolecular proton transfer. J Mol Struct THEOCHEM 910:27–33
18. Karaman R (2009) The *gem*-disubstituent effect-computational study that exposes the relevance of existing theoretical models. Tetrahedron Lett 50:6083–6087
19. Karaman R (2010) Effects of substitution on the effective molarity (EM) for five membered ring-closure reactions- a computational approach. J Mol Struct THEOCHEM 939:69–74
20. Karaman R (2009) Analyzing Kirby's amine olefin – a model for amino-acid ammonia lyases. Tetrahedron Lett 50:73047309

21. Karaman R (2010) The effective molarity (EM) puzzle in intramolecular ring-closing reactions. J Mol Struct THEOCHEM 940:70–75
22. Karaman R (2010) The efficiency of proton transfer in Kirby's enzyme model, a computational approach. Tetrahedron Lett 51:2130–2135
23. Karaman R (2010) Proximity vs Strain in ring-closing reactions of bifunctional chain molecules- a computational approach. J Mol Phys 108:1723–1730
24. Karaman R (2010) The effective molarity (EM) – a computational approach. Bioorg Chem 38:165–172
25. Karaman R (2010) A general equation correlating intramolecular rates with “attack" parameters distance and angle. Tetrahedron Lett 51:5185–5190
26. Karaman R, Alfalah S (2010) Multi transition states in SN2 intramolecular reactions. Int Rev Biophys Chem 1:14–23
27. Karaman R, Pascal R (2010) A computational analysis of intramolecularity in proton transfer reactions. Org Biomol Chem 8:5174–5178
28. Karaman R, Hallak H (2010) Anti-malarial pro-drugs- a computational aided design. Chem Biol Drug Design 76:350–360
29. Karaman R (2010) Prodrugs of aza nucleosides based on proton transfer reactions. J Comput Mol Des 24:961–970
30. Hejaz H, Karaman R, Khamis M (2011) Computer-assisted design for paracetamol masking bitter taste prodrugs. J Mol Model. doi:10.1007/s00894-011-1040-5
31. Bruice TC, Pandit UK (1960) The effect of geminal substitution ring size and rotamer distribution on the intramolecular nucleophilic catalysis of the hydrolysis of monophenyl esters of dibasic acids and the solvolysis of the intermediate anhydrides. J Am Chem Soc 82:5858–5865
32. Bruice TC, Pandit UK (1960) Intramolecular models depicting the kinetic importance of “Fit” in enzymatic catalysis. Proc Natl Acad Sci USA 46:402–404
33. Milstein S, Cohen LA (1970) Concurrent general-acid and general-base catalysis of esterification. J Am Chem Soc 92:4377–4382
34. Milstein S, Cohen LA (1970) Rate acceleration by stereopopulation control: models for enzyme action. Proc Natl Acad Sci USA 67:1143–1147
35. Milstein S, Cohen LA (1972) Stereopopulation control I. Rate enhancement in the lactonizations of o-hydroxyhydrocinnamic acids. J Am Chem Soc 94:9158–9165
36. Menger FM, Ladika M (1990) Remote enzyme-coupled amine release. J Org Chem 35:3006–3007
37. Menger FM, Ladika M (1988) Fast hydrolysis of an aliphatic amide at neutral pH and ambient temperature. A peptidase model. J Am Chem Soc 110:6794–6796
38. Menger FM (1985) On the source of intramolecular and enzymatic reactivity. Acc Chem Res 18:128–134
39. Menger FM, Chow JF, Kaiserman H, Vasquez PC (1983) Directionality of proton transfer in solution. Three systems of known angularity. J Am Chem Soc 105:4996–5002
40. Menger FM (1983) Directionality of organic reactions in solution. Tetrahedron 39:1013–1040
41. Menger FM, Grosssman J, Liotta DC (1983) Transition-state pliability in nitrogen-to-nitrogen proton transfer. J Org Chem 48:905–907
42. Menger FM, Galloway AL, Musaev DG (2003) Relationship between rate and distance. Chem Commun 2370–2371
43. Menger FM (2005) An alternative view of enzyme catalysis. Pure Appl Chem 77:1873–1876, and references therein
44. Brown RF, van Gulick NM (1956) The geminal alkyl effect on the rates of ring closure of bromobutylamines. J Org Chem 21:1046–1049
45. Galli C, Mandolini L (2000) The role of ring strain on the ease of ring closure of bifunctional chain molecules. Eur J Org Chem 3117–3125 and references therein
46. Kirby A J, Parkinson A (1994) Most efficient intramolecular general acid catalysis of acetal hydrolysis by the carboxyl group. J Chem Soc Chem Commun 707–708.
47. Brown CJ, Kirby AJ (1997) Efficiency of proton transfer catalysis Intramolecular general acid catalysis of the hydrolysis of dialkyl acetals of benzaldehyde. J Chem Soc Perkin Trans 2:1081–1093
48. Craze GA, Kirby AJ (1974) The hydrolysis of substituted 2-methoxymethoxybenzoic acids. J Chem Soc Perkin Trans 2:61–66
49. Barber SE, Dean KES, Kirby AJ (1999) A mechanism for efficient proton-transfer catalysis. Intramolecular general acid catalysis of the hydrolysis of 1-arylethyl ethers of salicylic acid. Can J Chem 792–801
50. Kirby AJ, de Silva MF, Lima D, Roussev CD, Nome F (2006) Efficient intramolecular general acid catalysis of nucleophilic attack on a phosphodiester. J Am Chem Soc 128:16944–16952
51. Kirby AJ, Williams NH (1994) Efficient intramolecular general acid catalysis of enol ether hydrolysis. Hydrogen-bonding stabilization of the transition state for proton transfer to carbon. J Chem Soc Perkin Trans 2:643–648
52. Kirby AJ, Williams NH (1991) Efficient intramolecular general acid catalysis of vinyl ether hydrolysis by the neighbouring carboxylic acid group. J Chem Soc Chem Commun 1643–1644
53. Hartwell E, Hodgson DRW, Kirby AJ (2000) Exploring the limits of efficiency of proton-transfer catalysis in models and enzymes. J Am Chem Soc 122:9326–9327
54. Kirby AJ (1997) Efficiency of proton transfer catalysis in models and enzymes. Acc Chem Res 30:290–296
55. Asaad N, Davies JE, Hodgson DRW, Kirby AJ (2005) The search for efficient intramolecular proton transfer from carbon: the kinetically silent intramolecular general base-catalysed elimination reaction of o-phenyl 8-dimethylamino-1-naphthaldoximes. J Phys Org Chem 18:101–109
56. Kirby AJ, Lancaster PW (1972) Structure and efficiency in intramolecular and enzymatic catalysis Catalysis of amide hydrolysis by the carboxy-group of substituted maleamic acids. J Chem Soc Perkin Trans 2:1206–1214
57. Kirby AJ, Hollfelder F (2009) From Enzyme Models to Model Enzymes. R Soc Chem, 1st edn, pp 1–273
58. http://www.gaussian.com.
59. Casewit CJ, Colwell KS, Rappé AK (1992) Application of a universal force field to main group compounds. J Am Chem Soc 114:10046–10053
60. Murrell JN, Laidler KJ (1968) Symmetries of activated complexes. Trans Faraday Soc 64:371–377
61. Muller K (1980) Reaction paths on multidimensional energy hypersurfaces. Angew Chem Int Edn Engl 19:1–13
62. Cancès MT, Mennucci B, Tomasi J (1997) A new integral equation formalism for the polarizable continuum model: theoretical background and applications to isotropic and anisotropic dielectrics. J Chem Phys 107:3032–3041
63. Mennucci B, Tomasi J (1997) Continuum solvation models: A new approach to the problem of solute’s charge distribution and cavity boundaries. J Chem Phys 106:5151–5158
64. Mennucci B, Cancès MT, Tomasi J (1997) Evaluation of solvent effects in isotropic and anisotropic dielectrics and in ionic solutions with a unified integral equation method: Theoretical bases, computational implementation, and numerical applications. J Phys Chem B 101:10506–10517
65. Tomasi J, Mennucci B, Cancès MT (1997) The IEF version of the PCM solvation method: an overview of a new method addressed

to study molecular solutes at the QM ab initio level. J Mol Struct THEOCHEM 464:211–226
66. Katagi T (1990) AM1 study of acid-catalyzed hydrolysis of maleamic (4-amino-4-oxo-2-butenoic) acids. J Comput Chem 11:1094–1100
67. Burker U, Allinger NL (1982) Molecular Mechanics. American Chemical Society, Washington DC, USA
68. Dafforn A, Koshland DE Jr (1971) Theoretical aspects of orbital steering. Proc Natl Acad Sci USA 68:129–139
69. Kirby AJ (2005) Effective molarities for intramolecular reactions. J Phys Org Chem 18:101–278
70. It should be noted that DFT calculations in the presence of a mixture of acid and water are not feasible